The Astrophysical Journal, 743:205 (11pp), 2011 December 20 doi:10.1088/0004-637X/743/2/205

O AND Ne IN AN H–He FAST SOLAR WIND

H. S. Byhring[1], R. Esser[1], and Ø. Lie-Svendsen[2]
[1] Department of Physics and Technology, University of Tromsø, NO-9037 Tromsø, Norway; hanne-sigrun.byhring@uit.no
[2] Norwegian Defense Research Establishment, P.O. Box 25, NO-2027 Kjeller, Norway
Received 2011 August 9; accepted 2011 September 7; published 2011 December 6

ABSTRACT

We have studied the abundances and ion fractions of O and Ne in an H–He fast solar wind with emphasis on gravitational settling in the chromosphere and corona. We use a time-dependent numerical model that spans the mid- to upper chromosphere, transition region, corona, and solar wind and calculates the particle density, flow velocity, parallel and perpendicular temperature, and heat flux for all particle species simultaneously. We investigate the effect of including He on the O and Ne abundances in the solar wind for two different flux tube expansion factors and find that He has a modest effect, which nevertheless becomes important for low expansion factors. The He, O and Ne abundances in the solar wind can be modulated by varying the magnetic flux tube expansion factor, but we have not been able to reproduce the observed solar wind abundances of He, O and Ne simultaneously. Furthermore, we find that unless O is heated to temperatures higher than those observed in polar coronal holes, there will be an O abundance enhancement in the corona, at about 1.6 $R_{\odot}$. Finally, we find that we can reproduce the in situ ion fractions for O and Ne in H–He background solutions with a modest He heating rate, which implies a coronal He abundance of about 20–40%.

Key words: Sun: abundances – Sun: corona – Sun: chromosphere

Online-only material: color figures

1. INTRODUCTION

In models of minor ion properties in the fast solar wind, the ions are usually treated as test particles in an H (proton–electron) background. To our knowledge, the only study which has treated minor ions in an H–He background is that of Bürgi & Geiss (1986), which focused on reproducing in situ ion fractions for several minor ions. They found that it was necessary to include He in the background in order to obtain ion fractions in accordance with observations in the solar wind. They also found that friction with He had a significant impact on the minor element outflow velocity and that an He abundance enhancement in the corona would lead to coronal abundance enhancements for the minor species. However, no attempt was made to study the minor element ion fractions and abundances as a function of the magnitude of the He abundance enhancement. In addition, the model of Bürgi & Geiss (1986) was based on several simplifications, some of which are problematic when modeling the behavior of minor ions. For example, the study assumed equal temperatures for all species, an assumption which is clearly not in accordance with observations, especially for polar coronal holes (e.g., Antonucci et al. 2000; Kohl et al. 1999; Esser et al. 1999; Cranmer et al. 1999; Wilhelm et al. 1998; see also Figure 1). Furthermore, the model of Bürgi & Geiss (1986) has its lower boundary in the low corona, which means that the energy balance in the transition region and chromosphere is not properly treated (e.g., Withbroe 1988; Lie-Svendsen et al. 2002) and that effects such as gravitational settling in the chromosphere, which may be of importance for minor element abundances in the corona and solar wind, are not treated in the model. In this paper, we study the properties of O and Ne in an H–He fast solar wind with particular emphasis on gravitational settling in the corona, and the resulting elemental abundances.

The He abundance in the fast solar wind is usually observed to be around 40–60% lower than the photospheric He abundance (Bame et al. 1977; Wang 2008). A possible explanation for this is gravitational settling in the chromosphere. In this scenario, the solar wind He flux is determined by the force balance in the chromosphere and is proportional to the chromospheric H flux, which in turn depends on the degree of flux tube expansion between the photosphere and 1 AU. A large flux tube expansion leads to a large H flux in the chromosphere which means that the frictional drag on neutral He in the chromosphere, through collisions with H and protons, is large, ensuring a solar wind He abundance close to the photospheric abundance. For a low flux tube expansion, the frictional drag is reduced and the solar wind will be severely depleted of He. Using the neutral He momentum equation, Lie-Svendsen et al. (2003) obtained an analytical expression for the largest possible He flux in the solar wind and found that an expansion factor of 15 or larger would be necessary to obtain a reasonable He flux in the solar wind. This result was confirmed by Byhring (2011) who found that a flux tube expansion of about 20 was sufficient to obtain a solar wind He abundance of 5% (Bame et al. 1977; Wang 2008), given a photospheric abundance of 8.5% (Asplund et al. 2009).

According to von Steiger et al. (2000) the heavy, high-first ionization potential (FIP) element Ne is also depleted in the solar wind, with respect to the photosphere. Pucci et al. (2010) used a model of the upper chromosphere to investigate the fractionation of O, Ne, and Fe as a function of the chromospheric H flux, or alternatively the flux tube expansion. They found that the observed solar wind Ne abundance places the strongest constraint on the flux tube expansion, an expansion factor of about 40 was needed to pull a sufficient amount of Ne out into the solar wind. However, in the model of Pucci et al. (2010) He was not included. Even if the He abundance in the chromosphere is never larger than 10%, He is four times heavier than H and the collisional drag from He may therefore be important. In the first part of this paper we will investigate the effect of the collisional drag from He on the solar wind abundances of O and Ne and we will study the O and Ne abundances as function of the flux tube expansion factor in an H–He background.

Coronal He abundance enhancements have been studied theoretically by several authors (e.g., Byhring 2011; Janse et al. 2007; Lie-Svendsen et al. 2003; Hansteen et al. 1997; Li et al.

1997; Bürgi & Geiss 1986) and can be understood in terms of heating and gravitational settling. In the low corona the collisional coupling between H and He (in the form of protons and alpha particles) is strong, ensuring approximately equal flow velocities for the two species. As the proton and He temperatures increase and the density decreases further out in the corona, the collisional coupling becomes weaker and the He flow velocity must adjust itself so that the friction force, together with the pressure gradient force, can balance gravity. Since the friction force is proportional to the velocity difference between He and H, the He flow velocity must decrease relative to the H velocity (assuming $u_{\rm He} < u_{\rm H}$, which holds in the corona for nearly all of our modeled cases). When the He velocity decreases relative to the H velocity, mass conservation dictates that the He density must increase relative to the H density, i.e., that a local He abundance enhancement must form. However, if the He ions are strongly heated the resulting large He pressure ensures that the friction force, and hence, the velocity difference between He and H, does not need to be so large (it can even be reversed, so that $u_{\rm He} > u_{\rm H}$, in which case there will be no He abundance enhancement). Hence, the magnitude of the He abundance enhancement will depend on the He heating rate in the corona. A large He abundance in the corona will affect the properties of minor elements as well as protons and electrons.

Lie-Svendsen & Esser (2005) studied elemental abundance enhancements in the corona for O and Si in an H fast solar wind. They found that elemental abundance enhancements will occur if the minor ions are not heated sufficiently in the corona. In the second part of this paper we aim to investigate how, and if, the magnitude of a coronal He abundance enhancement will influence the magnitude and location of minor ion abundance enhancements in the corona. We will use O as an example, since the response to changes in the H–He background will be similar for O and Ne. By varying the O heating rate in the corona, we can also determine whether a coronal O abundance enhancement will exist for O temperatures and flow speeds in accordance with observations in coronal holes (Antonucci et al. 2000; Kohl et al. 1999; Esser et al. 1999; Cranmer et al. 1999). Since observations of outflow velocity and temperature exist over a range of heights in the corona for O^{+5}, O is particularly well suited for comparisons between modeling and observations of the coronal O abundance.

For high He heating rates, the flow velocity of the H–He background may become large (see Section 3.1). For high flow velocities, the minor ions may be pushed far out of ionization equilibrium in the corona. We will determine the frozen-in ion fractions of O and Ne for different He heating rates and compare them to in situ observations. In this way, we may be able to place some constraints on the He heating rate in the corona and the magnitude of the coronal He abundance.

1.1. Abundances

As mentioned in Section 1, the He abundance in the fast solar wind is usually observed to be around 40–60% lower than the photospheric He abundance (Bame et al. 1977; Wang 2008). The photospheric He abundance can be established with great accuracy through helioseismology. A recent review by Asplund et al. (2009) lists a value of $N_{\rm He}/N_{\rm H} = 0.085 \pm 0.002$. In our simulations we use an He abundance at the lower boundary equal to the photospheric abundance.

The He abundance in the corona, on the other hand, is not well known. Over the years, many attempts have been made to determine the coronal He abundance (e.g., Gabriel et al. 1995; Raymond et al. 1997; Laming & Feldman 2001, 2003), however this has proved difficult partly because of the low intensity of relevant emission lines in the corona, especially in polar coronal holes, and partly because of the complex nature of the excitation mechanisms of the emission lines (e.g., Laming & Feldman 2001, 2003, and references therein). Laming & Feldman (2003) estimate the coronal He abundance by comparing the He II Baγ λ1085 emission line with emission lines from O VI, N V, and C IV. To estimate the He abundance from the observations Laming & Feldman (2003) assume ionization equilibrium and photospheric abundances for O, N, and C. Under these assumptions they find that the He abundance on open field lines, in the region below 1.1 $R_\odot$, never exceeds 5%. Our simulation results for O^{+5} and He^{+1} confirm that the assumption of ionization equilibrium is valid for outflow velocities of order 10 km s^{-1} in the region 1.03–1.1 $R_\odot$, which is in good accordance with observations of O^{+5} blueshift by Peter & Judge (1999). Byhring (2011) showed that for coronal proton densities and temperatures in accordance with observations, He abundance enhancements in the corona will occur well above 1.1 $R_\odot$.

The photospheric O abundance can be estimated by observations of neutral O emission lines. A summary of the results of various studies can be found in the review by Asplund et al. (2009), who recommend a value of $N_{\rm O}/N_{\rm H} = 4.9 \times 10^{-4}$. The coronal O abundance has been measured in a polar coronal hole by Antonucci & Giordano (2001), who obtained a value of $N_{\rm O}/N_{\rm H} = 6 \times 10^{-4}$ at the average height of 1.64 $R_\odot$. It is usually assumed that O is not fractionated with respect to H, since they have equal first ionization potentials. Pucci et al. (2010) demonstrate that this assumption may be invalid. They find that for low flux tube expansions O will be depleted by a factor 2–3 relative to the photosphere. Interestingly enough, the value recommended by Asplund et al. (2009) for the photospheric O abundance is lower than the observed O abundance in the corona and in the fast solar wind ($N_{\rm O}/N_{\rm H} = (6\text{–}7) \times 10^{-4}$; von Steiger et al. 1995, 2010). This seems to suggest that O is not depleted relative to the photosphere, but is in fact enhanced. We will not speculate on how this may come about, we simply assume that in the mid-chromosphere, at the lower boundary of our model, the O abundance is $N_{\rm O}/N_{\rm H} = 6.6 \times 10^{-4}$ in accordance with the results of von Steiger et al. (2010).

The photospheric Ne abundance is highly debated. A summary of recent results can be found in Asplund et al. (2009). The value adopted by them is based on their calculations of the photospheric O abundance and a recent study of the Ne/O abundance ratio by Young (2005). Young (2005) uses observations of transition region lines in the quiet Sun to arrive at $N_{\rm Ne}/N_{\rm O} = 0.17$, which gives $N_{\rm Ne}/N_{\rm H} = 0.85 \times 10^{-4}$ using the O abundance of Asplund et al. (2009), and argues that this value should be used also for the photosphere. However, Killie & Lie-Svendsen (2007) demonstrated that for a quiescent coronal loop, the transition region O abundance is far from equal to the chromospheric/photospheric O abundance. Since the force balance in the transition region will be different for O and Ne, we should not assume that the ratio of the abundances of the two elements is the same in the transition region and in the photosphere/chromosphere. The recent revisions of photospheric abundances adopted in Asplund et al. (2009) have led to discrepancies between models of the solar interior and results from helioseismology. Antia & Basu (2005) suggested that the discrepancies might be resolved by increasing the photospheric Ne abundance. Bahcall et al. (2005) suggested a value

of $N_{Ne}/N_H = 1.95 \times 10^{-4}$. We conclude that the photospheric Ne abundance is not well known, and that the value suggested by Bahcall et al. (2005) should be taken as an upper limit.

In the fast solar wind von Steiger et al. (2000) found a value of $N_{Ne}/N_O = 0.083$ for the Ne abundance. If we adopt the fast wind O abundance of von Steiger et al. (2010), this gives us an Ne abundance of $N_{Ne}/N_H = 0.55 \times 10^{-4}$.

2. MODEL

The model used in this study is based on the gyrotropic transport equations of Janse et al. (2005) and it builds on the models developed earlier by Hansteen & Leer (1995) and Lie-Svendsen et al. (2001). The model extends from the mid-chromosphere (1.0014 $R_\odot$, i.e., 1000 km above the photosphere) to 1 AU and calculates the radial profile of the plasma density, the flow velocity, the parallel and perpendicular temperature, and the heat flux along the magnetic field for each particle species. The input parameters to the model are the heating rates for the particles and the shape of the magnetic flux tube. The pressure and location of the transition region adjusts itself so that the radiative losses in the transition region, together with the energy required to heat the upwelling plasma, balance the heat conducted down from the corona, meaning that the mass flux of the solar wind is determined by our choice of heating parameters (Hansteen & Leer 1995). Ionization, recombination and charge exchange between particle species is included in the model and we do not assume ionization equilibrium.

At the lower boundary we assume an H density of $n_H = 10^{20}$ m^{-3} and an He density of $n_{He} = 8.5 \times 10^{18}$ m^{-3} (i.e., an He abundance of 8.5% in accordance with Asplund et al. 2009). The area of the flux tube at the lower boundary is 1 m^2. The temperature and flow velocity at the lower boundary adjusts itself according to the input parameters. The chromospheric temperature is kept at a value of 7000–8000 K by a chromospheric heating term which is adjusted so as to balance the radiation loss.

We assume optically thin radiative loss given by $n_e n_H f(T)$, where n_H is the actual neutral H density obtained in the code. The loss function $f(T)$ is taken from Judge & Meisner (1994). See Lie-Svendsen et al. (2001) for details.

The equations are solved first for the H–He "background," in which the minor species (O and Ne) can be treated as test particles. The He ions are not treated as test particles, which means that they are allowed to affect the properties of H/protons (e.g., through friction).

The protons, electrons, and alpha particles are heated by a prescribed energy flux which is exponentially damped. The proton and alpha particle heating starts at $r = 1.03\,R_\odot$ and the energy is deposited over a distance of about $2\,R_\odot$. Both He and H are fully ionized at $r = 1.03\,R_\odot$, where the heating is switched on, and therefore only protons and alpha particles are heated. The protons and alpha particles are only heated in the perpendicular direction. The electron heating starts at $r = 1.0\,R_\odot$ and the energy is deposited within $1.5\,R_\odot$. The heating of electrons is isotropic. The heating parameters have been chosen so as to produce plasma parameters that match existing observations from coronal holes. Since the focus of this study is the minor elements, a parameter study for the background species, with the aim of placing constraints on the heating parameters based on coronal observations, is outside the scope of this study. It is possible that a different set of heating parameters may produce similar results.

For the minor ions we apply a given heating rate per particle defined as

$$Q_{sm} = \begin{cases} 0 & r < r_1, \\ Cn_s \dfrac{r - r_1}{r_2 - r_1} \exp\left(-\dfrac{r - R_\odot}{H_m}\right) & r_1 < r < r_2, \\ Cn_s \exp\left(-\dfrac{r - R_\odot}{H_m}\right) & r > r_2, \end{cases} \quad (1)$$

where $R_\odot$ is the solar radius and n_s is the density of species s. The minor ion heating begins at a heliocentric distance of $r = r_1$ and is ramped up linearly to its full value at $r = r_2$. This is done to avoid numerical problems which may arise when the heating is switched on suddenly. Above this height the heating is damped with a damping length of H_m. The heating rate coefficient, C, can be specified individually for all the different charge states. The minor ions are heated only in the perpendicular direction.

The cross-sectional area of the flow tube is given by (Kopp & Holzer 1976)

$$A(r) = A_0 \left(\frac{r}{R_S}\right)^2 f_1(r) f_2(r), \quad (2)$$

where $A_0 = 1$ m^2 is the area of the flow tube at the solar surface, and

$$f_i(r) = \frac{f_{\max i} \exp\left[\frac{r - R_{1i}}{\sigma_i}\right] + f_{1i}}{\exp\left[\frac{r - R_{1i}}{\sigma_i}\right] + 1}, \quad (3)$$

where

$$f_{1i} = 1 - (f_{\max i} - 1) \exp\left[\frac{R_\odot - R_{1i}}{\sigma_i}\right]. \quad (4)$$

$f_i(r)$ is the expansion function and describes the expansion of the flow tube as a function of radial distance. The expression for the cross-sectional area of the flow tube allows for non-radial expansion in two different regions along the flow tube, around R_{11} and R_{12}. At $R_{11}(R_{12})$, the cross-sectional area of the flow tube increases to $f_{\max 1}(f_{\max 1} f_{\max 2})$ times the area of a radially expanding flow tube, and most of the increase occurs in the region $R_{11} - \sigma_1$ to $R_{11} + \sigma_1 (R_{12} - \sigma_2$ to $R_{12} + \sigma_2)$. The maximum value of $\frac{\partial f_i}{\partial r}$ occurs at R_{1i}. In our background models, $f_{\max 1} = 4, 10$, $f_{\max 2} = 10$, $R_{11} = 1.01 R_S$, $R_{12} = 2 R_S$, $\sigma_1 = 0.005 R_S$, and $\sigma_2 = 1 R_S$.

The model equations, details of the numerical scheme and information about the atomic data used in the simulations, can be found in Janse et al. (2005, 2007), Lie-Svendsen et al. (2001), and Hansteen & Leer (1995). The rates for the production and loss of the O and Ne charge states due to electron collisions, and recombinations have been obtained from the High Altitude Observatory Spectral Diagnostic Package for emitted radiation (HAOS-DIAPER; Judge & Meisner 1994).

In the chromosphere we use the collision frequency from Schunk (1977). For collisions between particle species s and t, with mass m_s and m_t, density n_s and n_t, and temperature T_s and T_t we have

$$\nu_{st} = \frac{8}{3\sqrt{(\pi)}} \frac{n_t m_t}{m_s + m_t} \left(\frac{2kT_{st}}{\mu_{st}}\right)^{1/2} \pi \sigma^2, \quad (5)$$

where $T_{st} = (m_t T_s + m_s T_t)/(m_s + m_t)$, $\mu_{st} = (m_s + m_t)/m_s m_t$, k is the Boltzmann constant, and $\pi\sigma^2$ is the hard sphere cross section. The expression in Equation (5) can be rewritten as

$$\nu_{st} = \frac{8}{3}\sqrt{(2\pi k \mu_{st} T_{st})}\sigma^2 \cdot \frac{n_t}{m_s} = g(\mu_{st}, T_{st}) \cdot \frac{n_t}{m_s}. \quad (6)$$

Table 1
The Values used for $g(\mu_{st}, T_{st})$ and σ (from Peter 1998) in the Model

Elements	$g(\mu_{st}, T_{st})$ (kg m^{-3} s^{-1})	σ (Å)
H, He	2.00×10^{-42}	1.56
H, Ne	2.62×10^{-42}	1.75
H, O	4.28×10^{-42}	2.26
He, Ne	4.91×10^{-42}	1.75
He, O	8.02×10^{-42}	2.26

Since the chromospheric temperature is the same for all species and does not vary significantly between the different solutions, we can calculate $g(\mu_{st}, T_{st})$ and use the simplified expression from Equation (6) in the code. The obtained values of $g(\mu_{st}, T_{st})$ used in the model are listed in Table 1 together with the values used for σ (Peter 1998).

We have not found any estimates of σ for collisions with between O/Ne and He in the literature. Therefore, we have chosen to use the values listed for H–O and H–Ne collisions. This small inaccuracy should not have a significant impact on the results of our simulations.

3. RESULTS

3.1. The H–He Background Solutions

To study the properties of Ne and O in an H–He fast solar wind, we have constructed four different background solutions. To study the variation of minor element abundances as function of the flux tube expansion factor, we will use one H–He solution with an expansion factor of 40 (named exp40) and one with an expansion factor of 100 (named exp100).

To study how coronal minor element (in this case O) abundance enhancements are affected by He, we will use three H–He background solutions: (1) the exp100 solution, (2) a solution with a lower He heating rate and a more pronounced coronal He abundance enhancement (named exp100.lo), and (3) a solution with a higher He heating rate and a smaller coronal He abundance enhancement (named exp100.hi).

The heating parameters for all four solutions are listed in Table 2. To make solutions exp40 and exp100 comparable, the total amount of heating has been scaled according to the expansion factor. Since the area of the flux tube in exp100 is 2.5 times larger than the area of the flux tube in exp40 (except in a very narrow region at the bottom), the energy supply to exp100 must be 2.5 times larger than the energy supply to exp40 to provide the same solar wind energy flux density at 1 AU. In addition to the direct heating of the plasma particles, energy is also supplied to the plasma in the form of Alfvén wave momentum deposition. The Alfvén wave energy flux density at the lower boundary is also listed in Table 2. At 1 AU, the Alfvén wave energy flux has been reduced by about 95%. The resulting proton flux density and He abundance at 1 AU is also listed in Table 2.

Figure 1 shows (a) the magnetic field expansion, (b) the proton flow speed, (c) the electron density, and (d) the proton perpendicular and electron temperature for the solutions in Table 2. The match to existing observations is good for all four H–He solutions. Figure 2 shows (a) the coronal He abundance, (b) the flow speed ratio between alpha particles and protons, and (c) the ratio between the perpendicular temperatures of alpha particles and protons.

Table 2
Energy Flux Deposited in the Protons, Alpha Particles, and Electrons for the Solutions Plotted in Figure 1

Solution	exp100	exp100.lo	exp100.hi	exp40
Model input:				
Protons (W m^{-2})	3000	3000	2967	1204
Alphas (W m^{-2})	1300	650	3933	516
Electrons (W m^{-2})	2250	2250	2250	900
Alfvén waves (W m^{-2})	4000	4000	4000	1600
Model output:				
$n_p u_p$ (m^{-2} s^{-1})	1.76×10^{12}	1.59×10^{12}	2.03×10^{12}	1.78×10^{12}
n_{He}/n_H	8.2%	8.1%	7.6%	7.2%

Notes. Also listed is the proton flux density and He abundance at 1 AU. Energy deposition has been scaled according to the expansion factor to make solutions comparable. For more details, see Section 2.

As expected from the discussion in Section 1, the exp100.lo solution has the largest coronal abundance enhancement and the exp100.hi solution has the smallest. In Figure 2 we also see that the height of the abundance enhancement varies according to the amount of He heating; for higher heating rates the abundance enhancement moves to lower heights. In Section 1 it was stated that the abundance enhancement occurs as a result of a weakening in the collisional coupling between protons and alpha particles that is due, in part, to increasing proton and alpha particle temperatures in the corona. The proton and alpha particle temperatures increase more rapidly when the heating rate is high, as in exp100.hi, causing the abundance enhancement to occur at lower heights.

As discussed by Li et al. (1997), when the He ions are heated at low heights, where the collisional coupling to the protons and electrons is good, heat will be transferred from the alpha particles to the protons and electrons and then conducted down to the chromosphere. Consequently, when the He heating increases, more energy will be conducted down to the chromosphere and the transition region pressure and the coronal density will increase. As a result, there will be less energy available per proton in the corona and the proton flow velocity here decreases.

However, if the He ions are heated above the region where they are well coupled to the protons and electrons, as is the case in our solutions, more of the energy deposited into the He fluid will be used to heat and accelerate the He ions. Nevertheless, some of the energy inserted into the He ions will be transferred to the protons through collisions. Thus, when the He heating rate is increased, the proton temperature also increases. From Figure 1 we can see that the proton perpendicular temperature at 1.2 $R_\odot$ increases from 1.3 MK in exp100.lo to 1.9 MK in exp100.hi. When the proton and alpha particle temperatures increase, the coupling between alphas, protons, and electrons becomes weaker and less energy will be transferred from the ions to the electrons. This means that less energy will be conducted by the electrons down to the chromosphere, and the transition region will move upward to a region of lower pressure, consistent with a lower coronal density. As a result, there will be more energy available per proton in the corona and the flow velocity here increases. In addition, the increased He flow velocity means that the frictional drag on the protons is reduced, or even reversed (i.e., He pulls protons away from the Sun) if the He flow speed exceeds that of the protons (as in exp100.hi). This also leads to an increase in the proton

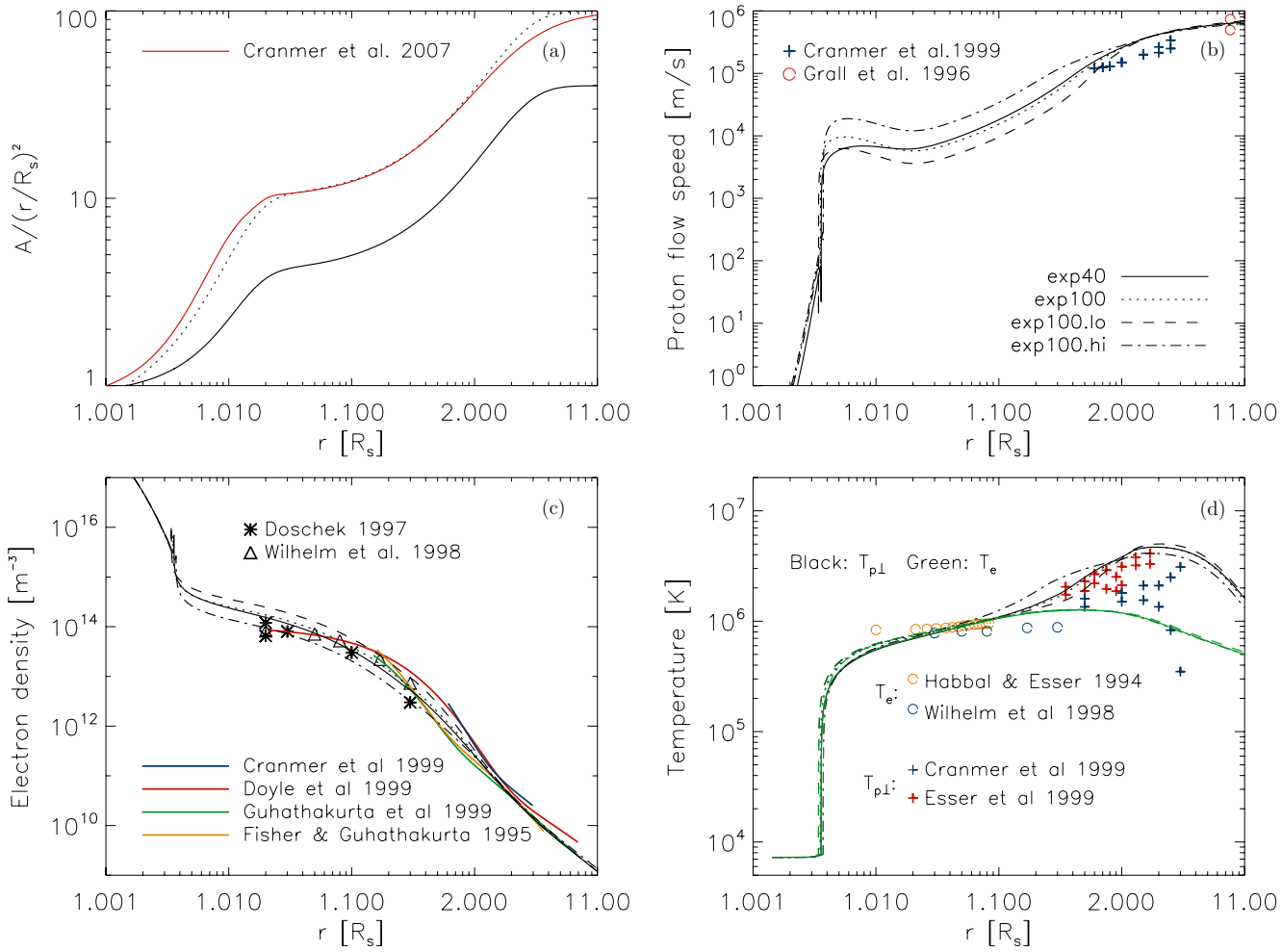

Figure 1. Proton–electron plasma parameters in models exp40, exp100, exp100.lo, and exp100.hi. (a) Flux tube expansion, (b) flow velocity, (c) electron density, and (d) proton and electron temperatures.

(A color version of this figure is available in the online journal.)

flow velocity. From Figure 1 we can see that the proton flow speed at 1.2 $R_\odot$ increases from about 20 km s^{-1} in exp100.lo to almost 80 km s^{-1} in exp100.hi and the coronal density decreases correspondingly, from 5×10^{12} m^{-3} in exp100.lo to 1.5×10^{13} m^{-3} in exp100.hi.

3.2. Ne and O in the Chromosphere

In this section we will first plot and discuss the results from the Ne and O simulations in the exp40 background to illustrate the behavior of these two minor elements in the chromosphere. We will then show how the solar wind Ne and O abundances depend on the flux tube expansion factor. Figure 3 shows the abundances (upper panel) and the flow speed ratios (lower panel) of Ne (solid line) and He (dotted line) obtained in the exp40 background plotted as a function of height in the first 0.005 $R_\odot$ of the model, corresponding to the chromosphere, transition region, and part of the low corona. The flow speed ratio is the ratio between the average velocities of Ne/He and H, where the average is taken over all charge states. We find that the Ne abundance increases in the upper chromosphere and then decreases sharply in the transition region.

We can explain this behavior by studying the Ne flow speed ratio. In the chromosphere, where Ne is in the neutral state, the Ne flow velocity is determined by a force balance between gravity and friction. The friction force, which is a sum of two components, friction from H and from He, is proportional to the flow speed difference between Ne and the background particle species. (As we can see in Figure 3, the He flow speed is close to the H flow speed throughout the chromosphere.) Below the transition region, the collisional coupling results from neutral–neutral collisions and is weak. Therefore, the flow speed difference between Ne and the background species must be large in order for the friction force to balance gravity. As the background density decreases toward the upper chromosphere, the collisional coupling between Ne and the background decreases. To compensate, and maintain force balance between gravity and friction, the flow speed difference between Ne and the background must increase. Conservation of mass flux requires that when the Ne flow speed decreases relative to H, the abundance must increase, hence the Ne abundance enhancement in the upper chromosphere. Above the transition region, where Ne is ionized, the strong Coulomb coupling to the background species ensures that the flow speed of Ne is approximately equal to that of H and He. As the Ne flow velocity increases relative to H through the transition region, mass conservation requires that the Ne abundance decreases. In Figure 3 we also see that at $r = 1.0035\ R_\odot$, there is a sharp peak in the flow speed ratios of He and Ne. This is a result of the strong acceleration of the heavy ions by the thermal force in the transition region.

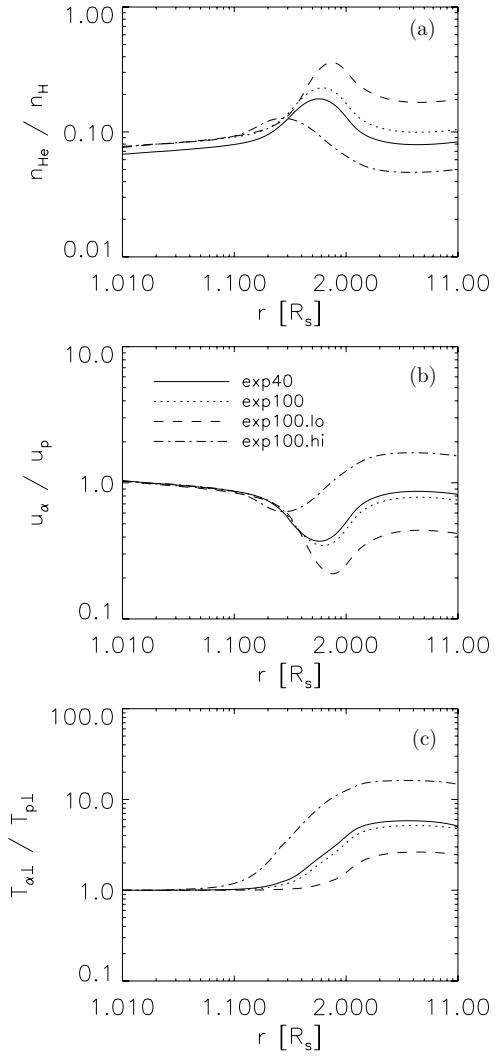

Figure 2. Coronal He abundance (a), ratio of alpha particle to proton speed (b), and ratio of alpha particle to proton perpendicular temperature (c) for all four background models in Table 2.

In the chromosphere, the component of the friction force which results from collisions with H constitutes about 90% of the total magnitude of the friction force. If He is removed from the exp40 background solution, we find that friction with H alone is not sufficient to balance gravity, even when the Ne outflow velocity is set to zero. As a result, there will be a downflow of Ne in the chromosphere, and the Ne density in the upper chromosphere will decrease until an upwardly directed pressure gradient force of sufficient magnitude has been set up which, together with the friction force, can balance gravity. In this case, the solar wind Ne flux in a steady state will be vanishingly small. We can use the analytical expression from Pucci et al. (2010) for the maximum possible absolute fractionation of an element i with mass m_i across a height interval in the chromosphere of thickness $z_u - z_l$:

$$\max(f[i]) = \frac{\frac{g}{\hat{\nu} F_H}\left(1 - \frac{m_p}{m_i}\right) - 1}{e^{\gamma\tau} - 1}, \tag{7}$$

where g is the gravitational acceleration, m_p is the proton mass, F_H is the hydrogen flux density and

$$\hat{\nu} \equiv \nu_{iH}/n_H, \tag{8}$$

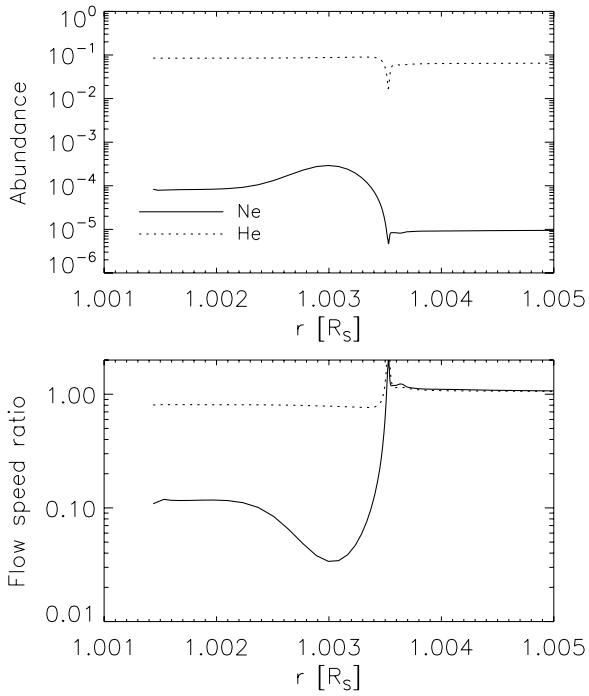

Figure 3. Abundance (upper panel) and flow speed ratio (lower panel) for Ne (u_{Ne}/u_H, solid lines) and He (u_{He}/u_H, dotted lines) in the chromosphere, transition region, and low corona for the exp40 background.

$$\gamma \equiv \frac{m_i}{m_p}\left(1 - \frac{\hat{\nu} F_H}{g}\right) - 1, \tag{9}$$

and

$$\tau \equiv \frac{m_p g (z_u - z_l)}{kT}, \tag{10}$$

where T is the (constant) chromospheric temperature in the slab $z_u - z_l$. The "effective" collision frequency ν_{iH} is found by taking into account that the element may be partially ionized. However, this is not necessary in the case of Ne, which is neutral throughout the chromosphere. Choosing $\hat{\nu} = \nu_{NeH}/n_H = 7.8 \times 10^{-17}$ m^3 s^{-1} (see Table 1) we find $g/\hat{\nu} = 3.5 \times 10^{18}$ m^{-2} s^{-1}, and taking $z_u - z_l = 1.5 \times 10^6$ m, $T = 7300$ K, and F_H equal to 2.6×10^{18} m^{-2} s^{-1} (from solution exp40) we find $\max(f[\mathrm{Ne}]) = 2 \times 10^{-13}$, i.e., the solar wind abundance will be no larger than $0.85 \times 10^{-4} \times 2 \times 10^{-13} = 1.7 \times 10^{-17}$ for a photospheric Ne abundance of 0.85×10^{-4}.

Starting from the Ne solution shown in Figure 3, we find that after 280 hr the Ne abundance in the exp40 background (with only H) has reached 2×10^{-7} and is still dropping.

In the exp100 background, on the other hand, the chromospheric H outflow velocity is higher than the flow speed difference, $u_H - u_{Ne}$, which is required for the friction force from collisions with H alone to balance gravity, meaning that in this solution Ne will not be trapped in the chromosphere if He is removed from the background. We find that in the exp100 background, the effect of removing He from the background is small.

Figure 4 is similar to Figure 3 and shows the abundance (upper panel) and the flow speed ratios (lower panel) of neutral O (solid line, only plotted in the chromosphere) and ionized O (dotted line) in the exp40 background with (black lines) and without (green lines) He included in the background. The flow velocity in the chromosphere is significantly higher for O compared to Ne. This is mainly a result of charge exchange collisions between H and O which increase the collisional coupling between these

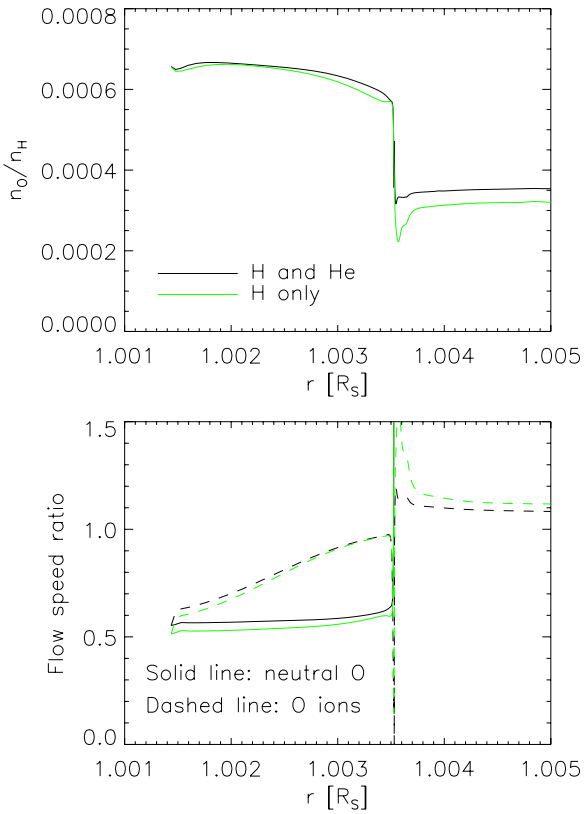

Figure 4. Abundance (upper panel) and flow speed ratio (with respect to H, lower panel) for neutral O (solid lines) and ionized O (dashed lines) in the chromosphere, transition region, and low corona for the exp40 background (black) and exp40 without He (green).

(A color version of this figure is available in the online journal.)

two species. Since the collisional coupling to the background is stronger, a lower flow speed difference between O and H is required to maintain the force balance between gravity and friction. As the ion fractions of protons and O^{+1} increase in the upper chromosphere, both reaching a value of 0.07 at 0.0035 $R_\odot$, the coupling between H and O due to charge exchange collisions improves, the average O flow speed (not shown) increases relative to the H flow speed, and the O abundance drops to lower values. As in the case of Ne there is a drop in the O abundance through the transition region, but it is much smaller. We find that removing He from the background does not lead to a large change in the O solution. This is another consequence of the strong coupling between H and O that results from charge exchange collisions.

By assuming mass conservation for H and a minor element species, i, and equal flow velocities above the transition region, it is easy to show that if the minor element abundance at the lower boundary is equal to A, then the minor element abundance above the transition region is equal to

$$\frac{n_i}{n_{\rm H}} = A \cdot \left(\frac{u_i}{u_{\rm H}}\right)_{\rm LB}, \qquad (11)$$

i.e., proportional to the velocity ratio at the lower boundary. If the H (and He) flow velocity in the chromosphere is large, then the flow speed difference between the minor element and the background species can be large even for $\frac{u_i}{u_{\rm H}} \sim 1$. If, on the other hand, the flow speed of the background species is low, then the flow speed difference that is required to balance gravity will result in a low $\frac{u_i}{u_{\rm H}}$. The flow velocity of the background species in the chromosphere depends on the magnetic field expansion factor, where high expansion factors lead to high velocities in the chromosphere.

Table 3
Obtained Solar Wind Abundances for Ne and O

Elements	Expansion	Abundance at Lower Boundary (10^{-4})	Solar Wind Abundance (10^{-4})
H, He, Ne	40	0.85 (1.95)	0.1 (0.23)
H, He, Ne	100	0.85 (1.95)	0.55 (1.3)
H, He, O	40	6.6	4.0
H, He, O	100	6.6	5.7

Notes. All abundances are relative to H. For Ne, the abundance obtained with $N_{\rm Ne}/N_{\rm H} = 0.85 \times 10^{-4}$ at the lower boundary is listed outside parentheses and the abundance obtained with $N_{\rm Ne}/N_{\rm H} = 1.95 \times 10^{-4}$ at the lower boundary is listed inside parentheses. Solutions number 1 and 3 were plotted in Figures 3 and 4 in the previous section.

Table 4
Solutions with O in Different Backgrounds and with Different Heating Rates

Solution	Background	Peak $n_{\rm O}/n_{\rm H}$	Height of Peak $n_{\rm O}/n_{\rm H}$ ($R_\odot$)	C (10^{-19} W)
1	exp100	0.0028	1.68	5
2	exp100.lo	0.0043	1.64	5
3	exp100.hi	0.0031	1.8	5
4	exp100, H only	0.0048	1.57	5
5	exp100.lo	0.0026	1.54	30
6	exp100.hi	0.0015	1.66	30

The abundances O and Ne obtained with the exp40 and exp100 backgrounds are listed in Table 3. Also listed is the assumed abundance at the lower boundary. Since the minor ions are treated as test particles, the Ne abundance can be scaled up or down without affecting the shapes of the radial profiles for density, velocity, temperature, and heat flux obtained in each solution. Given the existing uncertainty about the photospheric Ne abundance, we list two values for the Ne abundance in Table 3. The numbers listed outside parentheses are obtained using an Ne abundance at the lower boundary of $N_{\rm Ne}/N_{\rm H} = 0.85 \times 10^{-4}$ and the numbers listed inside parentheses are obtained with an Ne abundance at the lower boundary of $N_{\rm Ne}/N_{\rm H} = 1.95 \times 10^{-4}$ (see Section 1.1).

As was shown in Figure 3, the Ne abundance in the exp40 background decreases by almost an order of magnitude in the transition region. In the exp100 background the abundance decreases by only about 35%. In the case of O we find that the difference between the exp40 and the exp100 backgrounds is much smaller than for Ne. Nevertheless, a reduction in the O abundance between the chromosphere and the corona/solar wind is present in both the exp40 and the exp100 backgrounds.

3.3. The Corona–Local Abundance Enhancements

To study the effect of He on coronal minor element abundance enhancements that occur as a result of low heating rates (Lie-Svendsen & Esser 2005), we will use O as an example.

We have created six O solutions, four with a low O heating rate (1–4) and two with a high O heating rate (5–6). In the solution where He is not present (solution 4) we have used the H parameters from exp100 as the background solution. The solutions are described in Table 4. The applied heating in solutions 1–4 is not sufficient to achieve observed O^{+5} temperatures and outflow velocities, but in solutions 5–6 the observed O^{+5}

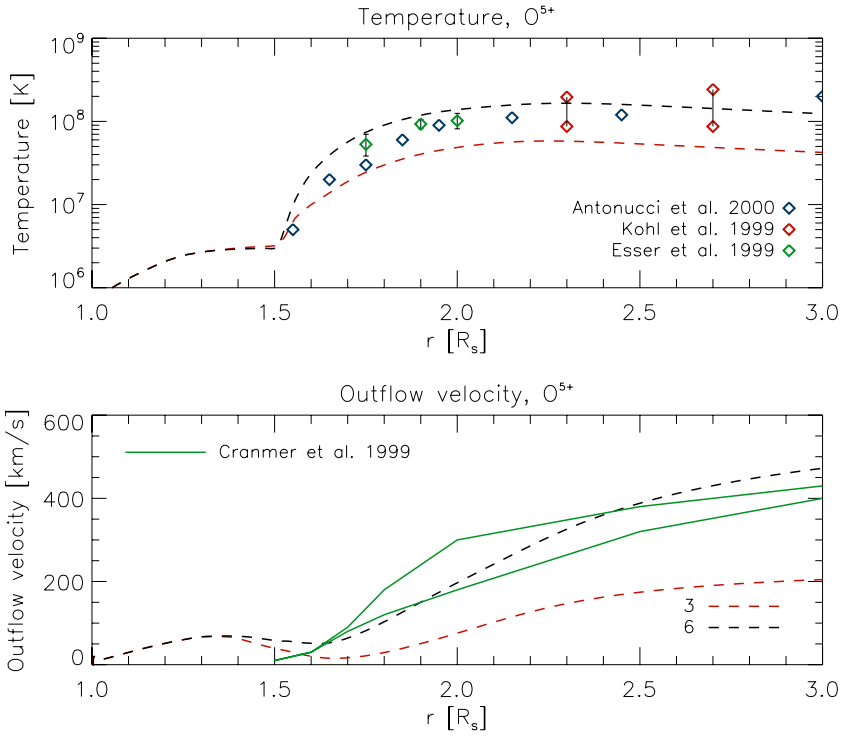

Figure 5. Temperature (upper panel) and outflow velocity (lower panel) of O^{+5} in the corona in solutions 3 and 6 from Table 4.
(A color version of this figure is available in the online journal.)

temperatures and outflow velocities are approximately reproduced (see Figure 5, where we have used solutions 3 and 6 as examples). In all six solutions the heating is switched on at $r = 1.1\ R_\odot$ (see Equation (1)) and is ramped up linearly until it reaches its maximum value at $r = 1.5\ R_\odot$. Above this height the heating rate decreases exponentially with a damping length of $1\ R_\odot$. The He and O abundances in the corona for the solutions in Table 4 are shown in Figure 6.

It is immediately clear from the figure that an O abundance enhancement in the corona is present, even in the solutions that do reproduce observed O^{+5} temperatures and outflow velocities.

When the He heating rate is reduced, the He abundance enhancement will become more pronounced. The friction force between He and O is proportional to $n_{\rm He}(u_{\rm He} - u_{\rm O})$, and when the He density increases the friction force is reduced (since $n_{\rm He}u_{\rm He}$ is approximately the same in all solutions, the change in the friction force is a result of the change in the second term, which is negative). However, the value of the friction force that is required to achieve force balance in the corona (where the O pressure gradient and friction force must balance gravity) is independent of the H–He background solution. To compensate for the reduction in the friction force that is caused by the increase in the He density, the O flow speed must decrease with the result that the O abundance enhancement increases in magnitude. The same argument can be made for the friction force between O and protons. Since the proton density increases when the He heating rate is reduced, and the friction force is proportional to $n_p(u_p - u_{\rm O})$, where $n_p u_p$ is more or less independent of the He heating rate, the friction force will be reduced. To compensate, the O flow speed must decrease.

In the above discussion we claimed that the proton and He flux densities were independent of the He heating rate. As can be seen from Table 2, this is not entirely correct. The proton flux density (and hence, also the He flux density) decreases

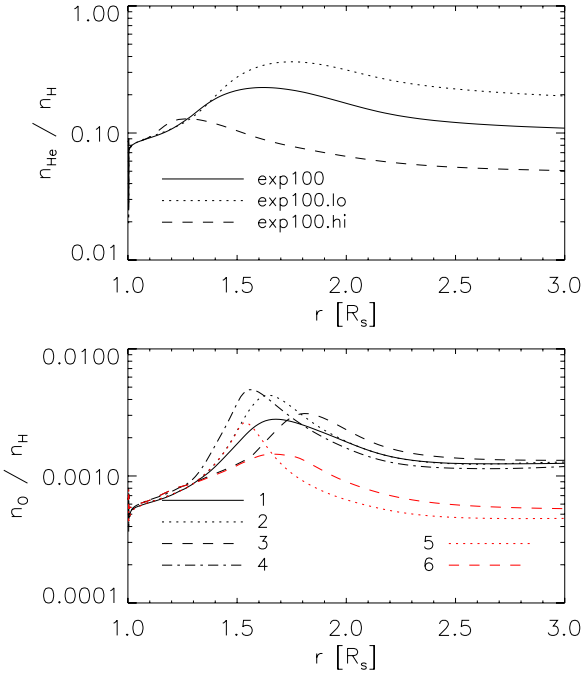

Figure 6. He (upper panel) and O (lower panel) abundance in the corona for background solutions exp100, exp100.lo, and exp100.hi, and for two different heating rates (see Table 4).
(A color version of this figure is available in the online journal.)

somewhat when the He heating rate is reduced. However, this will only add to the effect discussed above. If $n_{\rm He}u_{\rm He}$ and $n_p u_p$ is reduced, the result is a reduction in the friction force. To compensate, the O flow speed must decrease.

Finally, reducing the He heating rate leads to a decrease in the He temperature, i.e., to an increase in the degree of coupling

Table 5
Ion Fractions for O^{+5}, O^{+6}, and O^{+7} in Solutions 1–3

Solution	Background	O^{+5}	O^{+6}	O^{+7}
1	exp100	0.004	0.98	0.01
2	exp100.lo	0.004	0.98	0.02
3	exp100.hi	0.004	0.99	0.003

between He and O and therefore also to an increase in the magnitude of the friction force from collisions between He and O. To compensate, the O flow speed must now increase, reducing the flow speed difference between O and He, and thereby also the friction force and the O abundance enhancement. This can be illustrated by comparing solutions 1 and 3 in Figure 6. In solution 3, the small He abundance enhancement acts to reduce the magnitude of the O abundance enhancement, relative to solution 1, and the increased He temperature acts to increase the magnitude of the O abundance enhancement. The net result is that the O abundance enhancement in solution 3 moves to a higher altitude and increases in magnitude relative to solution 1.

The effect of including He in the background can be seen by comparing solutions 1 and 4. The O abundance enhancement occurs at a lower height and the peak O abundance is higher when He is removed from the background. When He is removed from the background, the component of the friction force that is caused by collisions between O and He disappears. To compensate for this the O flow velocity must be reduced so that the friction force caused by collisions with H increases. The reduction in the O flow velocity corresponds to an increase in the O abundance enhancement. As in the case of He, increasing the O heating rate, and thereby the O pressure, leads to a reduction in the O abundance enhancement (solutions 5 and 6). The results for Ne are very similar to those obtained for O and overall, the effect of He on O and Ne in the corona is small.

3.4. Ion Fractions for O and Ne at 1 AU

In Table 5 we have listed the ion fractions for O^{+6} and O^{+7} in solutions 1–3. The freezing-in height, above which the flux of each individual charge state is constant with respect to r (Hundhausen et al. 1968), is close to 2 $R_\odot$ for all three solutions, i.e., just above the coronal abundance enhancement. This is in good accordance with the results of Ko et al. (1997). According to Gloeckler & Geiss (2007), typical ion fractions for O^{+5}, O^{+6}, and O^{+7} in the high-speed wind are approximately 0.003, 0.98, and 0.015, respectively. Solutions 1 and 2 provide the best fit to these observations, with an O^{+7} ion fraction of 0.01 and 0.02, respectively. In all three solutions, O^{+7} is driven out of ionization equilibrium in the corona, but the effect is strongest in solution 3, since it has the highest flow velocity. In ionization equilibrium, the O^{+7} ion fraction has its maximum at about 1.4 $R_\odot$ where it reaches a value of 0.06 (for the electron temperature profiles obtained in this study). It is the flow velocity in the region below 1.4 $R_\odot$ which mainly determines the final value of the O^{+7} ion fraction at 1 AU. Above this height, only minor changes in the ion fraction can be seen. Since this is below the region where the O heating is applied, it follows that the O heating rate is not important for the final O^{+7} ion fraction at 1 AU. Consequently, we find that the ion fractions obtained in solutions 5 and 6 are exactly the same as in solutions 2 and 3, respectively.

To calculate the ion fractions and freezing-in height of Ne, we use background solutions exp100, exp100.lo, and exp100.hi and a heating rate coefficient for Ne equal to $C = 30 \times 10^{-19}$ W.

Table 6
Ion Fractions for Ne^{+7} and Ne^{+8} for Solutions 1–3

Solution	Background	Ne^{+7}	Ne^{+8}
1 Ne	exp100	0.02	0.98
2 Ne	exp100.lo	0.02	0.98
3 Ne	exp100.hi	0.08	0.92

In Table 6 we have listed the resulting ion fractions for Ne^{+7} and Ne^{+8}. As in the case of O, the low-speed solutions, exp100 and exp100.lo, produce the best fits to the observations of Gloeckler & Geiss (2007), who found that typical ion fractions for Ne^{+7} and Ne^{+8} in the high-speed wind are approximately 0.015 and 0.98, respectively. The ion fractions are frozen-in at about 2 $R_\odot$, as was the case for O. Based on the results for O, we do not expect the ion fractions to depend on the choice of heating rates.

4. DISCUSSION

The effect of including He in the exp100 background solution for Ne is an increase in the Ne flow velocity at the lower boundary of about 0.2 u_H, or 0.02 m s^{-1}. This is a very modest increase in the flow velocity, and for O, which is quite well coupled to H through charge exchange collisions, the effect is even smaller. However, when the flux tube expansion is reduced to lower values, the effect of He may become very important. In the exp40 background, the presence of He ensures that Ne escapes into the corona and solar wind. In this solution, when we remove the extra friction term caused by He–Ne collisions, the friction from H–Ne collisions alone cannot balance gravity and Ne is trapped in the chromosphere. However, as stated in Section 3.2, the component of the friction force which results from collisions with H constitutes about 90% of the total magnitude of the friction force in the chromosphere. So, if we increase the flux tube expansion factor from 40 to 44, the friction from H–Ne collisions is sufficient to balance gravity and there is no need for a strong Ne density gradient (i.e., a larger pressure gradient force) to form in the chromosphere.

As mentioned in Section 1, the results of Lie-Svendsen et al. (2003) and Byhring (2011) show that a flux tube expansion factor of about 15–20 yields an He abundance consistent with observations in the fast solar wind. In the present paper, all the H–He background solutions have expansion factors of 40 or more, and solar wind He abundances of more than 7% (see Figure 2), i.e., much larger than the observed value. However, as we have seen in Section 3.2, even an expansion factor of 40 is not sufficient to reproduce the observed solar wind Ne abundance.

Thus, it is clear that we are not able to reproduce the observed solar wind abundances of both He, O and Ne using a single flux tube expansion factor. Despite the uncertainties that still exist regarding the photospheric abundances of O and Ne, this is conclusive. However, that does not mean that the flux tube expansion factor is unimportant. As we have seen, the solar wind Ne abundance is strongly affected by the expansion factor, and this effect should be taken into account in models that aim to explain how the solar wind minor element abundances are determined. It is also well worth noting that O may be fractionated with respect to H in the solar wind, as was also shown by Pucci et al. (2010). The drag from H and He in the chromosphere is not sufficient to ensure that O is not depleted in the solar wind relative to the photosphere.

Furthermore, the study of Byhring et al. (2008) showed that a flux tube expansion factor of more than 20 is not consistent with observed blueshifts of the O IV, O V, and O VI emission lines (Peter & Judge 1999; Wilhelm et al. 1998). Given these discrepancies, it is necessary to examine the effects of any physical processes in the chromosphere which we have neglected in the model and which may be of importance for the minor element abundances.

One possible weakness in our model is that it does not include turbulent mixing processes in the chromosphere. If turbulent mixing occurs in the chromosphere, then this would counteract gravitational settling and we would not require a large expansion factor to obtain a solar wind Ne abundance in accordance with observations. This does not, however, settle the question of the O abundance, since mixing alone cannot produce an enhancement in the absolute abundance. Furthermore, a study of the He abundance in a closed coronal loop by Killie et al. (2005) shows that the presence of turbulent mixing processes in the chromosphere may also have problematic consequences. In a coronal loop, where the net outflow is zero, the density of each individual particle species will adjust itself according to its own scale height in the absence of turbulent mixing processes. This means that the densities of, e.g., He and Ne at the top of the chromosphere will be very low. Killie et al. (2005) showed that in a coronal loop which is anchored in a "well-mixed" chromosphere, where the He abundance in the upper chromosphere is kept close to the photospheric He abundance, the coronal He density will become comparable to the H density after 1–3 days. If, on the other hand, the chromosphere is allowed to be stratified, ensuring a very low He abundance at the top of the chromosphere, Killie et al. (2005) find that the coronal He abundance can be kept at lower values, in accordance with observations. Thus, the study of Killie et al. (2005) suggests that turbulent mixing processes are not important in the upper chromosphere. To assume that turbulent mixing processes are important in the chromosphere below coronal holes, but not in the chromosphere below coronal loops, would at least require some kind of observational or theoretical justification which, to the authors knowledge, does not exist at the time. We conclude that a more complete model of the chromosphere is needed in order to fully understand the changes in the He and minor element abundances that occur between the photosphere and the solar wind.

In the study of Laming (2009), in which a "well-mixed" chromosphere was assumed, it was found that the ponderomotive force owing to Alfvén waves that propagate through the chromosphere could result in fractionation of minor elements that is consistent with the FIP effect. The study also finds that depletions in the He and Ne abundance arise naturally when the ponderomotive force owing to Alfvén waves is taken into account. These results are promising although the validity of the assumption of a well-mixed chromosphere remains uncertain.

Recent observations with the *Hinode* and *Solar Dynamics Observatory* spacecrafts (De Pontieu et al. 2011) have revealed that fountain-like jets or spicules can accelerate plasma upward from the chromosphere and into the corona. If these jets are responsible for a significant part of the mass supply to the corona, then the explanation for the abundance variations between the photosphere and the corona/solar wind should be sought within a theoretical framework and a model which is also capable of describing the physics of these plasma jets. For this task a one-dimensional model, such as we have used in this work, is probably not sufficient for the chromosphere.

As can be seen from our results, the assumption that the abundance of O is the same in the photosphere, chromosphere, corona, and solar wind is not necessarily valid. Since we are not able to explain the observed O and Ne abundances in the solar wind, we cannot use the simulation results from this study to verify or discard the idea that the O abundance in the low corona is close to that of the photosphere, as implied in the observations of Laming & Feldman (2003), who used emission lines of He II and O VI to place constraints on the He abundance in the low corona. The validity of this approach therefore remains uncertain, at least in the case of O VI, although the assumption of ionization equilibrium does seem to be justified.

In Section 3.3 we saw that a local O abundance enhancement is present in the corona in all the H–He background solutions and for both high and low heating rates. It is possible that an abundance enhancement can be avoided, but it would require heating O to higher temperatures than those observed in polar coronal holes. Antonucci & Giordano (2001) found a value of $N_O/N_H = 6 \times 10^{-4}$ at the average height of 1.64 $R_\odot$ in a polar coronal hole, which is about the same as the solar wind O abundance. The O abundance enhancements we obtain from the model are located at approximately the same height and consequently we find much higher abundances here. However, as discussed in Antonucci & Giordano (2001), their results depend on the assumed plasma properties in the corona. Thus, the observations are consistent with an O abundance as high as 0.0014, which is closer to the abundances we obtain in our simulations. There is also the possibility of contamination from plume plasma, which may have a different coronal O abundance compared to interplume plasma. We conclude that the coronal O abundance is not well known and that local abundance enhancements may exist. As in the case of He, the abundance enhancements occur in the region above 1.1 $R_\odot$. The magnitude and location of the abundance enhancement will depend to some degree on the magnitude and location of the He abundance enhancement, but is mainly determined by the O heating rate.

The results from Section 3.4 shows that we are able to reproduce approximately the observed ion fractions of O^{+6}, O^{+7}, Ne^{+7}, and Ne^{+8} at least in the exp100 and exp100.lo background solutions. It is clear that the very high flow velocity of the exp100.hi background solution pushes the O and Ne ions far out of ionization equilibrium and the resulting ion fractions are not in accordance with the observations. This result suggests that He abundance enhancements may be common in the corona, since a coronal He abundance enhancement cannot be avoided without depositing considerable amounts of energy into the He ions, which leads to high outflow velocities for protons, alpha particles, and minor ions in the corona. To obtain a slower wind, without increasing the magnitude of the He abundance enhancement (i.e., without lowering the He heating rate), it would be necessary to increase the electron heating rate, thereby moving the transition region to a region of higher pressure, which would lead to a denser and slower wind. However, this would also lead to a higher mass flux, which is not in accordance with observations of the fast solar wind at 1 AU.

5. CONCLUSIONS

We find, in accordance with the results of Pucci et al. (2010), that gravitational settling in the chromosphere has a large impact on the solar wind Ne abundance. In the absence of turbulent mixing processes, a flux tube expansion factor of at least 40 is

required to obtain the observed solar wind Ne flux. The flux tube expansion factor has a significant impact also on the solar wind He abundance, but we have not been able to reproduce the solar wind abundances of both He and Ne simultaneously, i.e., with a single flux tube expansion factor.

We also find that unless the O ions are heated to higher temperatures than those observed in polar coronal holes, it is difficult to avoid a local abundance enhancement of O in the corona. The abundance enhancement occurs at about 1.6 $R_{\odot}$ in our simulations. The magnitude of the coronal O abundance enhancements depends weakly on the magnitude of the He abundance enhancement, but is mainly dependent on the O heating rate. Finally, we show that most of our solutions produce ion fractions at 1 AU in accordance with observations, with the exception of solutions with a very high flow velocity in the corona. Since a coronal He abundance enhancement cannot be avoided without depositing considerable amounts of energy into the He ions, something which leads to large outflow velocities for protons, alpha particles, and O ions in the corona, this last result suggests that He abundance enhancements may be common in the corona.

REFERENCES

Antia, H. M., & Basu, S. 2005, ApJ, 620, L129
Antonucci, E., & Giordano, S. 2001, in AIP Conf. Proc. 598, Joint SOHO/ACE workshop Solar and Galactic Composition, ed. R. F. Wimmer-Schweingruber (Melville, NY: AIP), 77
Antonucci, E., Giordano, S., & Dodero, M. A. 2000, Adv. Space Res., 25, 1923
Asplund, M., Grevesse, N., Sauval, A. J., & Scott, P. 2009, ARA&A, 47, 481
Bahcall, J. N., Basu, S., & Serenelli, A. M. 2005, ApJ, 631, 1281
Bame, S. J., Asbridge, J. R., Feldman, W. C., & Gosling, J. T. 1977, J. Geophys. Res., 82, 1487
Bürgi, A., & Geiss, J. 1986, Sol. Phys., 103, 347
Byhring, H. S. 2011, ApJ, 738, 172
Byhring, H. S., Esser, R., & Lie-Svendsen, Ø. 2008, ApJ, 673, L91
Cranmer, S. R., Kohl, J. L., Noci, G., et al. 1999, ApJ, 511, 481
De Pontieu, B., McIntosh, S. W., Carlsson, M., et al. 2011, Science, 331, 55
Doyle, J. G., Keenan, F. P., Ryans, R. S. I., Aggarwal, K. M., & Fludra, A. 1999, Sol. Phys., 188, 73
Esser, R., Fineschi, S., Dobrzycka, D., et al. 1999, ApJ, 510, L63
Fisher, R., & Guhathakurta, M. 1995, ApJ, 447, L139
Gabriel, A. H., Culhane, J. L., Patchett, B. E., et al. 1995, Adv. Space Res., 15, 63
Gloeckler, G., & Geiss, J. 2007, Space Sci. Rev., 130, 139
Grall, R. R., Coles, W. A., & Klinglesmith, M. T. 1996, in AIP Conf. Proc. 382, Proceedings of the Eigth International Solar Wind Conference: Solar Wind Eight, ed. D. Winterhalter, J. T. Gosling, S. R. Habbal, W. S. Kurth, & M. Neugebauer (Melville, NY: AIP), 108
Guhathakurta, M., Fludra, A., Gibson, S. E., Biesecker, D., & Fisher, R. 1999, J. Geophys. Res., 104, 9801
Habbal, S. R., & Esser, R. 1994, ApJ, 421, L59
Hansteen, V. H., & Leer, E. 1995, J. Geophys. Res., 100, 21577
Hansteen, V. H., Leer, E., & Holzer, T. E. 1997, ApJ, 482, 498
Hundhausen, A. J., Gilbert, H. E., & Bame, S. J. 1968, J. Geophys. Res., 73, 5485
Janse, Å. M., Lie-Svendsen, Ø., & Leer, E. 2005, J. Plasma Phys., 71, 611
Janse, Å. M., Lie-Svendsen, Ø., & Leer, E. 2007, A&A, 474, 997
Judge, P. G., & Meisner, R. W. 1994, in Third SOHO Workshop, Solar Dynamic Phenomena and Solar Wind Consequences, ed. J. J. Hunt (ESA SP-373, Vol. 3; Noordwijk: ESA), 67
Killie, M. A., & Lie-Svendsen, Ø. 2007, ApJ, 666, 501
Killie, M. A., Lie-Svendsen, Ø., & Leer, E. 2005, ApJ, 632, L155
Ko, Y.-K., Fisk, L., Geiss, J., Gloeckler, G., & Guhathakurta, M. 1997, Sol. Phys., 171, 345
Kohl, J. L., Esser, R., Cranmer, S. R., et al. 1999, ApJ, 510, L59
Kopp, R., & Holzer, T. 1976, Sol. Phys., 49, 43
Laming, J. M. 2009, ApJ, 695, 954
Laming, J. M., & Feldman, U. 2001, ApJ, 546, 552
Laming, J. M., & Feldman, U. 2003, ApJ, 591, 1257
Li, X., Esser, R., Habbal, S. R., & Hu, Y.-Q. 1997, J. Geophys. Res., 102, 17419
Lie-Svendsen, Ø., & Esser, R. 2005, ApJ, 618, 1057
Lie-Svendsen, Ø., Hansteen, V. H., & Leer, E. 2003, ApJ, 596, 621
Lie-Svendsen, Ø., Hansteen, V. H., Leer, E., & Holzer, T. E. 2002, ApJ, 566, 562
Lie-Svendsen, Ø., Leer, E., & Hansteen, V. H. 2001, J. Geophys. Res., 106, 8217
Peter, H. 1998, A&A, 335, 691
Peter, H., & Judge, P. 1999, ApJ, 522, 1148
Pucci, S., Lie-Svendsen, Ø., & Esser, R. 2010, ApJ, 709, 993
Raymond, J. C., Kohl, J. L., Noci, G., et al. 1997, Sol. Phys., 175, 645
Schunk, R. W. 1977, Rev. Geophys. Space Phys., 15, 429
von Steiger, R., Geiss, J., Gloeckler, G., & Galvin, A. B. 1995, Space Sci. Rev., 72, 71
von Steiger, R., Schwadron, N. A., Fisk, L. A., et al. 2000, J. Geophys. Res., 105, 27217
von Steiger, R., Zurbuchen, T. H., & McComas, D. J. 2010, Geophys. Res. Lett., 37, L22101
Wang, Y. 2008, ApJ, 683, 499
Wilhelm, K., Marsch, E., Dwivedi, B. N., et al. 1998, ApJ, 500, 1023
Withbroe, G. L. 1988, ApJ, 325, 442
Young, P. R. 2005, A&A, 444, L45